NANO · MICRO
small

Supporting Information

for *Small*, DOI 10.1002/smll.202308066

Prominent Structural Dependence of Quantum Capacitance Unraveled by Nitrogen-Doped Graphene Mesosponge

Rui Tang, Alex Aziz, Wei Yu, Zheng-Ze Pan, Ginga Nishikawa, Takeharu Yoshii, Keita Nomura, Erin E. Taylor, Nicholas P. Stadie, Kazutoshi Inoue, Motoko Kotani, Takashi Kyotani and Hirotomo Nishihara**

Supporting Information

Prominent structural dependence of quantum capacitance unraveled by nitrogen-doped graphene mesosponge

Rui Tang*, Alex Aziz, Wei Yu, Zheng-Ze Pan, Ginga Nishikawa, Takeharu Yoshii, Keita Nomura, Erin E. Taylor, Nicholas P. Stadie, Kazutoshi Inoue, Motoko Kotani, Takashi Kyotani, and Hirotomo Nishihara*

Experimental Section

Material synthesis

Nitrogen-doped carbon species

The nitrogen-doped carbon species was prepared by means of chemical vapor deposition (CVD) on Al_2O_3 nanospheres (2 g; ~Ø7 nm, TM300, Taimei Chemicals Co., Ltd., Japan). Acetonitrile was used as the carbon and nitrogen source. Ar (225 mL min^{-1}) was used as the carrier gas. The CVD temperature was maintained at 650 °C, and the template was heated to this temperature at a rate of 10 °C min^{-1} under an Ar atmosphere. CVD was carried out over 3 h, during which time acetonitrile (~27 mL min^{-1}) was added with Ar bubbling (225 mL min^{-1}). Subsequently, the temperature was increased to 900 °C at a heating rate of 10 °C min^{-1}; this temperature was held constant for 1 h to anneal the deposited carbon on the Al_2O_3 template. The Al_2O_3 template was then removed using hydrofluoric acid to leave the carbon shell (nitrogen-doped carbon mesosponge, N-CMS). N-GMS specimens were prepared by heating N-CMS at 1000, 1200, 1400, 1600, or 1800 °C under vacuum, we denoted N-GMS-1000, N-GMS-1200, N-GMS-1400, N-GMS-1600, and N-GMS-1800, respectively, based on their annealing temperature (Fig. S1).

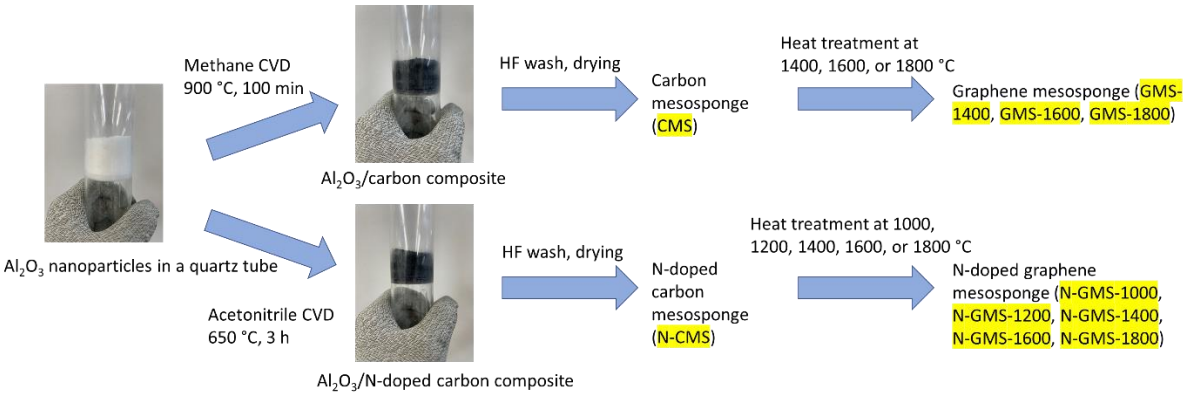

Fig. S1. Diagram of the materials synthesis process.

Undoped carbon reference materials

Al_2O_3 nanoparticles were used as the template on which a 3D graphene network was formed via the CVD of methane gas (45 mL min^{-1}) at 900 °C,[1-3] wherein Ar (180 mL min^{-1}) was used as the carrier gas. After heating the specimen to the target temperature of 900 °C at a heating rate of 10 °C min^{-1}, CVD was carried out for 100 min. The Al_2O_3 template was then removed using hydrofluoric acid to retain the carbon shell, which was denoted CMS. CMS was heated at 1400, 1600, or 1800 °C under vacuum to produce the samples denoted GMS-1400, GMS-1600, and GMS-1800, respectively.

General characterization

The amount of carbon deposited was measured by thermogravimetric (TG) analysis in air. The morphology of each nitrogen-doped carbon specimen was characterized using transmission electron microscopy (TEM, Titan^3 G2 60-300, Thermo Fisher Scientific, USA) and scanning electron microscopy (SEM, S-4800, Hitachi High-Tech Co., Ltd., Japan). The porosities of the carbon materials were determined by measuring their N_2 adsorption/desorption isotherms at −196 °C (BEL Japan, BELSORP MAX, Japan), while their specific surface areas (SSAs) were calculated by applying the Brunauer–Emmett–Teller (BET) theory to the adsorption isotherm (P/P_0 = 0.05–0.3). The pore size distributions were calculated using the nonlocal density functional theory (NLDFT) method applied to the adsorption isotherms. The carbon materials were also characterized by powder X-ray diffraction (XRD, MiniFlex600, Rigaku Co., Japan) with Cu Kα radiation generated at 40 kV and 15 mA. The Raman spectra were measured using a Jasco NRS-3300FL spectrometer (532.2 nm line), while X-ray photoelectron spectroscopy (XPS) was performed using a JPS-9200 (JEOL, Japan) instrument with Al Kα radiation generated at 10 kV and 10 mA. A CHN analyzer (J-Science Lab JM10 CHN, Japan) was employed to quantify the amounts of C, N, H, and O in each specimen.

Electrochemical measurements

The electrochemical performances of the mesoporous carbon materials were measured in an organic electrolyte (1 M Et_4NBF_4 in propylene carbonate) using a three-electrode cell. The working electrode (~5 mg) was fabricated by mixing the mesoporous carbon material, carbon black (Denka Black, Denka Co. Ltd., Japan), and a PTFE binder in an 80:5:15 weight ratio. The counter electrode (~10 mg) was prepared using the same method, with the exception that commercial activated carbon (YP-50F, Kuraray Chemical Co., Ltd., Japan) was used as the active material. $Ag/AgClO_4$ was used as the reference electrode. The open circuit potential (OCP) was measured after the stabilization of the three-electrode cell for 24 h. Using the cyclic voltammetry (CV) results obtained at 1 mV s^{-1}, the gravimetric capacitance was calculated based on the mass of a single electrode (C_{tot} [F g^{-1}]) as follows:

$$C_{\mathrm{tot}} = \frac{I\Delta t}{m\Delta V} = \frac{I}{m\frac{\Delta V}{\Delta t}}, \quad (1)$$

where I, Δt, m, ΔV, and $\Delta V/\Delta t$ represent the current [A], discharge time [s], carbon mass [g], potential change [V], and scan rate [V s^{-1}], respectively. The areal capacitance (C_{areal}, μF cm^{-2}) was calculated by normalizing to the SSA spanned by carbon as follows:

$$C_{areal} = \frac{C_{\mathrm{tot}}}{S_{\mathrm{BET}}}. \quad (2)$$

The C_H (μF cm^{-2}) value of the same organic electrolyte was also measured using Pt foil (0.02 mm × 20 mm × 20 mm, Nilaco Corporation, Japan) with the same three-electrode configuration as reported in our previous work.[4] All electrochemical measurements were performed at a constant temperature of 25 °C. The quantum capacitance (C_Q, μF cm^{-2}) was calculated as follows:

$$\frac{1}{C_{areal}} = \frac{1}{C_{\mathrm{H}}} + \frac{1}{C_{\mathrm{Q}}}. \quad (3)$$

It should be noted that C (F g^{-1}) can be used for comparison with activated carbon or other carbon materials. C_{areal} (μF cm^{-2}) and C_{Q} (μF cm^{-2}) were used for comparison with the results of previous theoretical calculations and experimental works[5-7] carried out on two-dimensional graphene.

Computational details

The nitrogen-doped systems were constructed from a 6 × 6 × 1 graphene supercell containing 72 atoms within the hexagonal setting and the (194) *P63/mmc* space group. For the pore systems, a slightly larger 8 × 8 × 1 supercell containing 128 atoms was used. The geometry of each system was optimized using the Vienna Ab initio Simulation Package (VASP)[8] with a cutoff energy of 520 eV for the plane-wave expansion. Brillouin zone integration was sampled using a 4 × 4 × 1 *k*-point Monkhorst-Pack grid for the nitrogen systems and a 3 × 3 × 1 grid for the pore systems. The generalized gradient approximation was used with the Perdew–Burke–Ernzerhof (PBE) exchange-correlation functional and the geometry relaxation stopping criteria was set to when the forces on all the atoms were less than 0.01 eV $Å^{-1}$.[9, 10] In addition, van der Waals (vdW) molecular interactions were included via the DFT-D3 method of Grimme with Becke-Johnson damping.[11] This gave a lattice parameter of 2.467 Å, close to the experimentally reported value for graphite 2.464 Å.[12] A 20 Å spacing perpendicular to the graphene surface was included to avoid interactions between periodic images as well as incorporate dipole corrections. The density of states (DOS) was calculated by first performing single-point calculations on the optimized geometry using a 6 × 6 × 1 *k*-point grid, then the DOS was calculated non-self-consistently using a fine 18 × 18 × 1 *k*-point grid. To obtain a meaningful comparison between the density of states of each system the Fermi energy was set to that of pristine graphene by calculating the vacuum electrostatic potential.[13] The capacitance curves were determined utilizing the JDFT*x* code, where JFDT stands for joint density-functional theory.[14] For our JDFT calculations, we used a *k*-point grid of 36 × 36 × 1 for pristine graphene and 6 × 6 × 1 for our nitrogen-doped systems and pore model. We incorporated a truncated Coulomb potential[15] and set the electronic convergence criteria to $<10^{-8}$ Hartrees using the PBE exchange-correlation functional where the atomic positions were optimized until the forces were less than 10^{-6} Hartree.[9, 10] A value of 20 Hartree was used for the electronic plan-wave expansion with a Fermi smearing value of 0.0005 Ha. The propylene carbonate (PC) solvent was modeled implicitly using the linear polarizable continuum model (LPCM)[16, 17] and by incorporating a 1 M concentration of anions and cations at a temperature of 298 K.

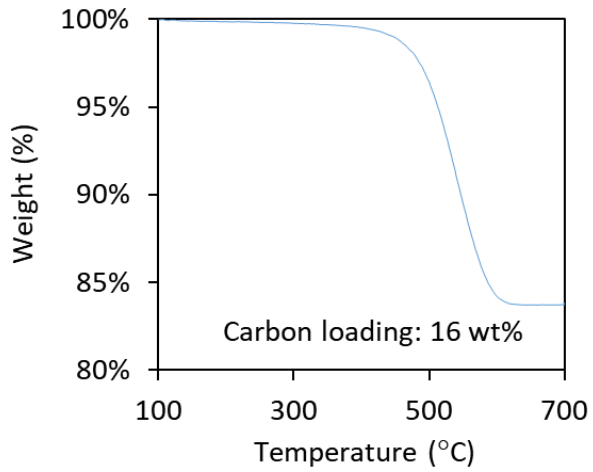

Fig. S2. TG analysis results for carbon-coated Al_2O_3 after CVD at 650 °C (3 h) with acetonitrile as the source of both carbon and nitrogen.

The average layer of the basal plane (N_{stack}) was calculated by the following equation:

$$N_{stack} = \frac{W_{carbon}}{S_{template} W_{graphene}} \quad (4)$$

where W_{carbon} is the weight of carbon deposited, $S_{template}$ is the SSA of the template heated at 650 °C (202 $m^2\ g^{-1}$). $W_{graphene}$ is the weight of graphene per unit area (7.614×10^{-4} g m^{-2}) calculated from its geometric structure.[1] N_{stack} was calculated to be 1.3.

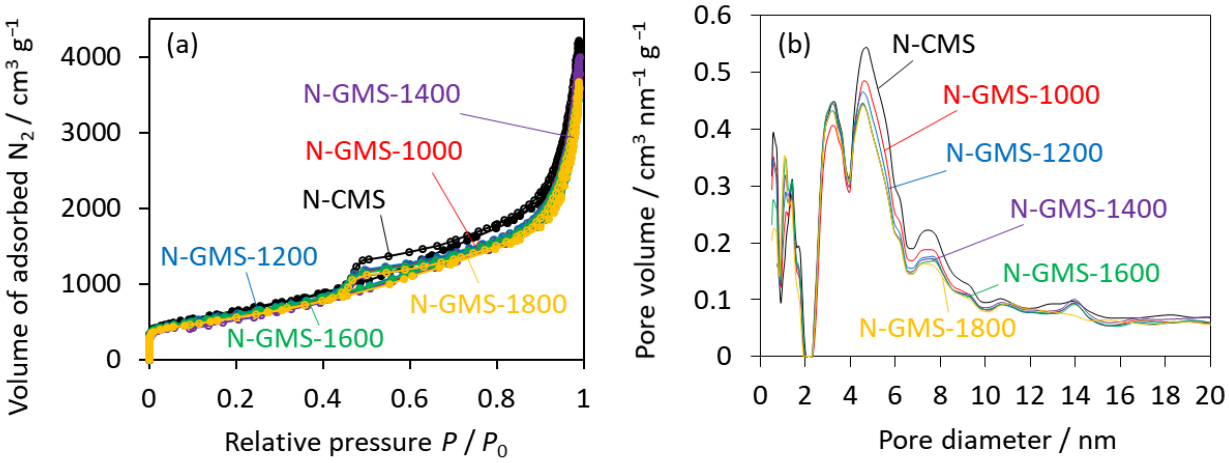

Fig. S3. (a) N_2 adsorption/desorption isotherms, and (b) pore size distributions of the prepared nitrogen-doped carbon materials.

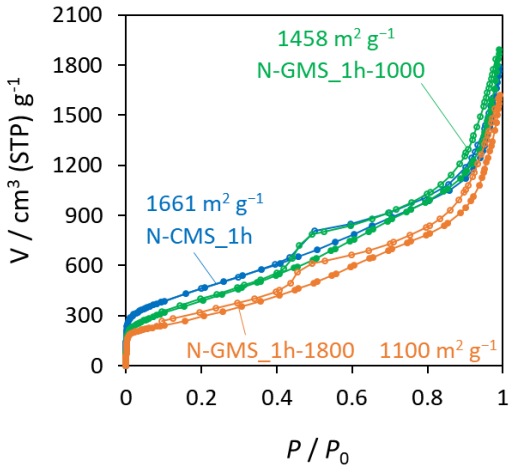

Fig. S4. N_2 adsorption/desorption isotherms the nitrogen-doped carbon materials prepared with a shorter CVD time of 1 h (denoted as N-CMS_1h) showed significantly reduced S_{BET} after high-temperature annealing (denoted as N-GMS_1h-1000 and N-GMS_1h-1800).

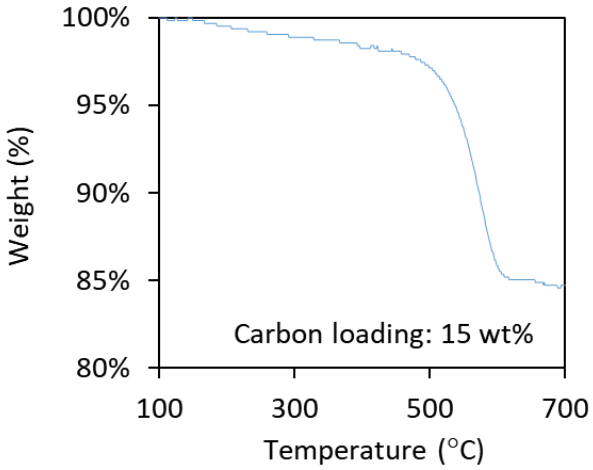

Fig. S5. TG analysis results for carbon-coated Al_2O_3 after CVD at 900 °C (100 min) with methane as the carbon source.

N_{stack} was calculated using Eq. (4), where $S_{template}$ is the SSA of the template heated at 900 °C (179 m^2 g^{-1}). N_{stack} was calculated to be 1.3.

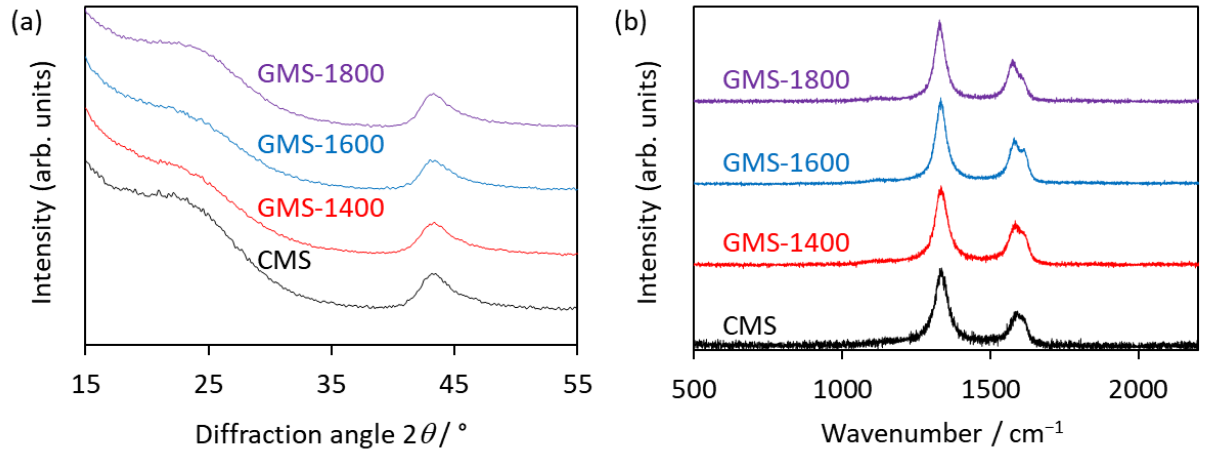

Fig. S6. (a) XRD and (b) Raman results for the undoped carbon species.

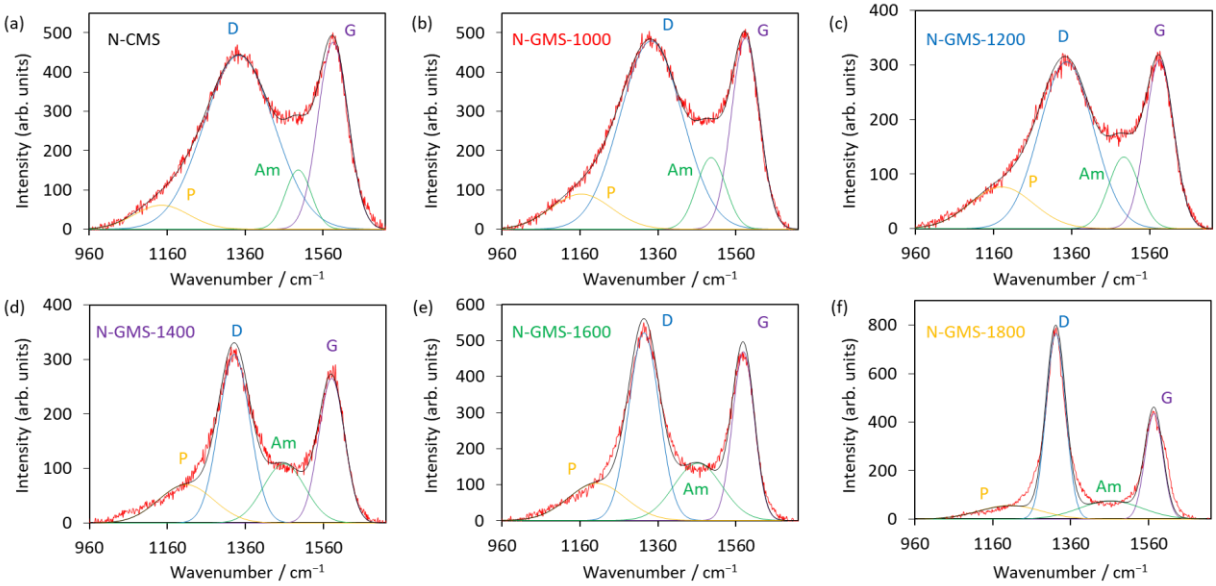

Fig. S7. Raman spectral deconvolutions for the (a) N-CMS, (b) N-GMS-1000, (c) N-GMS-1200, (d) N-GMS-1400, (e) N-GMS-1600, and (f) N-GMS-1800 specimens.

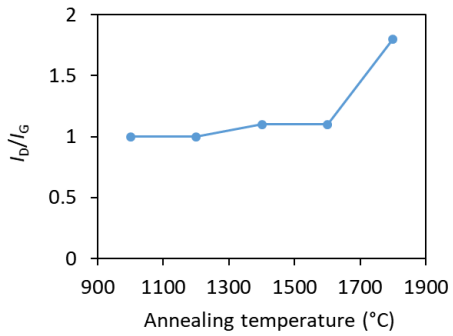

Fig. S8. The calculated I_D/I_G ratio for the nitrogen-doped carbon materials.

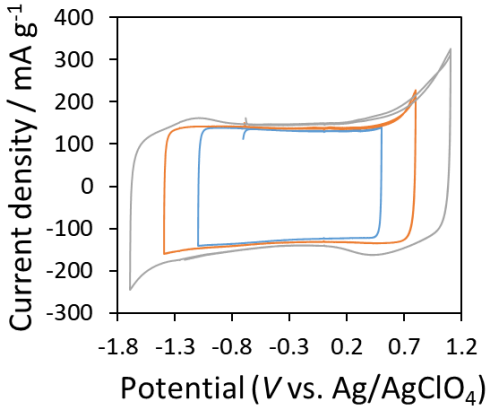

Fig. S9. CV curves of N-GMS-1000 measured at different potential windows.

When the potential window extends from 1.5 to 2.2 or 2.8 V as shown above (**Fig.** S9.), there is a rise of current in the extended potential ranges. However, this does not mean the increase of C_{tot} in these potential ranges but should be due to parasitic side reactions between carbon and organic solvent molecules.[18, 19] To correctly obtain C_{tot} and further calculate C_Q, we selected the limited potential window of 1.5 V.

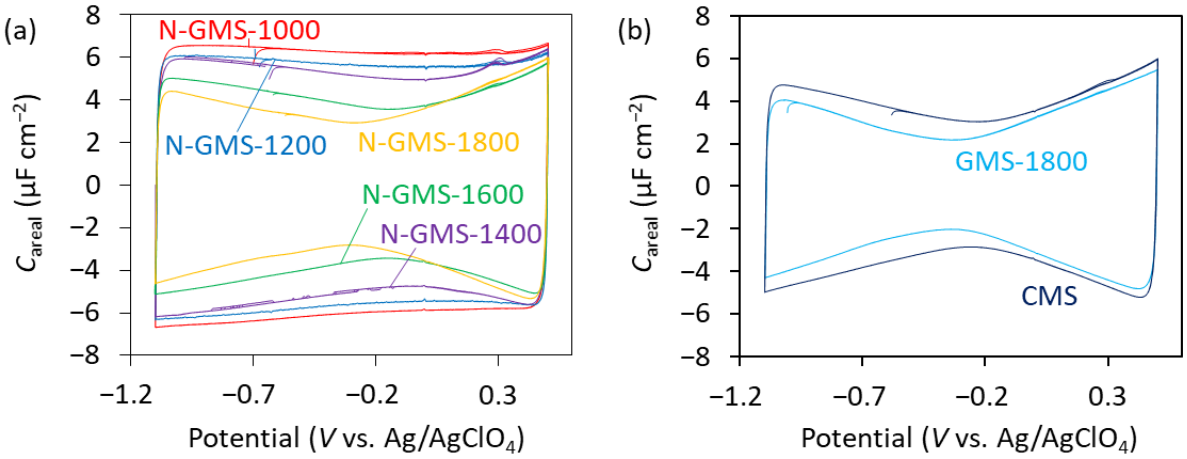

Fig. S10. Variation in the C_{areal} values with the applied potential for the (a) nitrogen-doped and (b) undoped carbon species.

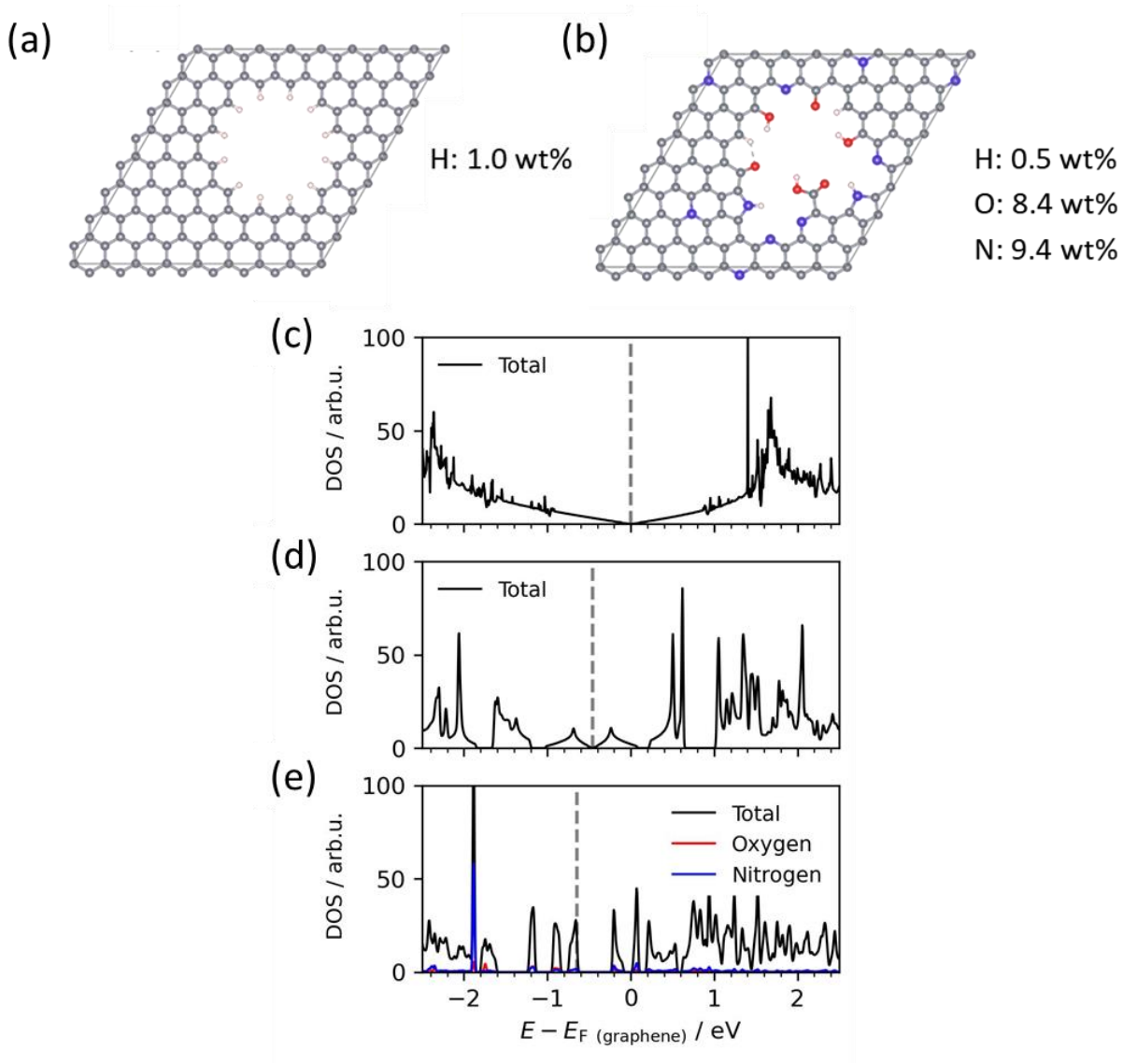

Fig. S11. Two hole-containing structural models: (a) Model 1 and (b) Model 2. Carbon, gray; hydrogen, pink; oxygen, red; and nitrogen, blue. DOS of the modeled systems (a) Pristine graphene, (b) Model 1, and (c) Model 2. Calculated using an 8 × 8 supercell. The Fermi level (dotted gray line) is referenced by setting the E_F of pristine graphene to 0 eV with the values calculated by determining the vacuum electrostatic potential.[13]

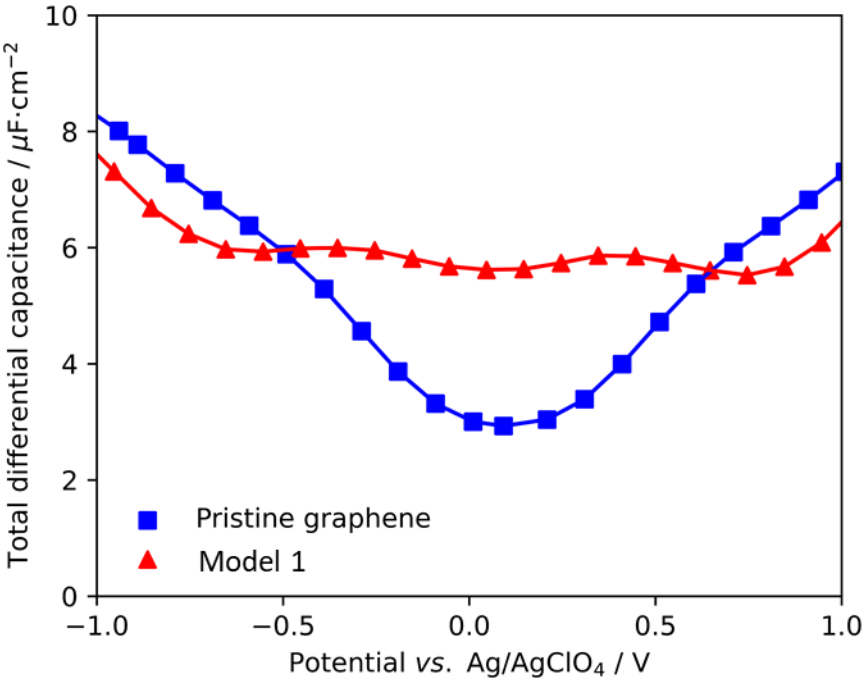

Fig. S12. C_{tot} calculated for Model 1 and pristine graphene.

References

1. H. Nishihara, T. Simura, S. Kobayashi, K. Nomura, R. Berenguer, M. Ito, M. Uchimura, H. Iden, K. Arihara, A. Ohma, Y. Hayasaka and T. Kyotani, *Adv. Funct. Mater.*, 2016, **26**, 6418-6427.
2. K. Nomura, H. Nishihara, N. Kobayashi, T. Asada and T. Kyotani, *Energy Environ. Sci.*, 2019, **12**, 1542-1549.
3. S. Sunahiro, K. Nomura, S. Goto, K. Kanamaru, R. Tang, M. Yamamoto, T. Yoshii, J. N. Kondo, Q. Zhao, A. Ghulam Nabi, R. Crespo-Otero, D. Di Tommaso, T. Kyotani and H. Nishihara, *J. Mater. Chem. A*, 2021, **9**, 14296-14308.
4. R. Tang, K. Nomura, K. Inoue, M. Kotani, T. Kyotani and H. Nishihara, *Electrochim. Acta*, 2022, **429**, 141009.
5. J. L. Xia, F. Chen, J. H. Li and N. J. Tao, *Nat. Nanotechnol.*, 2009, **4**, 505-509.
6. M. D. Stoller, C. W. Magnuson, Y. W. Zhu, S. Murali, J. W. Suk, R. Piner and R. S. Ruoff, *Energy Environ. Sci.*, 2011, **4**, 4685-4689.
7. J. F. Chen, Y. L. Han, X. H. Kong, X. Z. Deng, H. J. Park, Y. L. Guo, S. Jin, Z. K. Qi, Z. Lee, Z. H. Qiao, R. S. Ruoff and H. X. Ji, *Angew. Chem. Int. Ed.*, 2016, **55**, 13822-13827.
8. G. Kresse and J. Furthmüller, *Phys. Rev. Lett.*, 1996, **54**, 11169-11186.
9. J. P. Perdew, K. Burke and M. Ernzerhof, *Phys. Rev. Lett.*, 1996, **77**, 3865-3868.
10. B. C. Stipe, M. A. Rezaei, W. Ho, S. Gao, M. Persson and B. I. Lundqvist, *Phys. Rev. Lett.*, 1997, **78**, 4410-4413.
11. S. Ehrlich, J. Moellmann, W. Reckien, T. Bredow and S. Grimme, *ChemPhysChem*, 2011, **12**, 3414-3420.
12. P. Trucano and R. Chen, *Nature*, 1975, **258**, 136-137.
13. K. T. Butler, C. H. Hendon and A. Walsh, *J. Am. Chem. Soc.*, 2014, **136**, 2703-2706.

14. R. Sundararaman, K. Letchworth-Weaver, K. A. Schwarz, D. Gunceler, Y. Ozhabes and T. A. Arias, *SoftwareX*, 2017, **6**, 278-284.
15. R. Sundararaman and T. A. Arias, *Phys. Rev. B Condens. Matter Mater. Phys.*, 2013, **87**.
16. K. Letchworth-Weaver and T. A. Arias, *Phys. Rev. B Condens. Matter Mater. Phys.*, 2012, **86**.
17. D. Gunceler, K. Letchworth-Weaver, R. Sundararaman, K. A. Schwarz and T. A. Arias, *Model. Simul. Mater. Sci. Eng.*, 2013, **21**.
18. R. Tang, M. Yamamoto, K. Nomura, E. Morallón, D. Cazorla-Amorós, H. Nishihara and T. Kyotani, *J. Power Sources* 2020, **228042**.
19. R. Tang, K. Taguchi, H. Nishihara, T. Ishii, E. Morallón, D. Cazorla-Amorós, T. Asada, N. Kobayashi, Y. Muramatsu and T. Kyotani, *J. Mater. Chem. A* 2019, **7480**.